) 1 1
l 1 1
2 2 2
) 0 1
0 0]

) 0 0
) 0 0
) 0 0
2 1 1
0 2]

) 0 0
) 0 0
) 0 0
) 0 0
1 0]

Intermediate Species Profiles in Low Pressure Premixed Flames Inhibited by Fluoromethanes

DREW L'ESPÉRANCE,† BRADLEY A. WILLIAMS,* and JAMES W. FLEMING

Combustion Dynamics Section, Code 6185, Navy Technology Center for Safety and Survivability, Naval Research Laboratory, Washington, DC 20375-5342

We have investigated premixed 10 torr methane/oxygen flames containing CH_3F, CH_2F_2, CHF_3, and CF_4. Profiles of temperature and CH* chemi-luminescence were acquired, and laser-induced fluorescence (LIF) was used to obtain profiles of the intermediate species H, OH, CH, CF, CHF, CF_2, and CF_2O. The fluoromethanes were added in amounts such that each flame had the same flux of fluorine atoms. In the flames containing CH_3F, CH_2F_2, and CHF_3, the methane flow was adjusted to give an equivalence ratio of 1.07 for all three inhibited flames. The experimental intermediate profiles were compared to predicted profiles calculated from a hydrofluorocarbon kinetic mechanism recently developed at NIST. No fluorinated intermediates were detectable in the CF_4 inhibited flame, indicating that this agent does not react significantly under the flame conditions studied. The temperature profiles, H atom profiles, and OH profiles for the other three fluoromethane inhibited flames are nearly identical, indicating that flames containing different fluorocarbon compounds, but identical proportions of fluorine atoms, have similar structures. The kinetic model correctly predicts the location of the reaction zone in the flames containing CH_2F_2 and CH_3F. In the CHF_3 flame, however, the location of the reaction zone is predicted to be too far above the burner surface, and concentrations of H and OH are too low. The discrepancy appears to be due to pressure dependence and third body efficiencies of the agent thermal decomposition. Furthermore, relative amounts of CF, CH, CF_2, and CHF in the different flames are not very well predicted. In general, partially fluorinated methyl and methylene radicals appear to have a greater than predicted propensity to lose hydrogen atoms rather than fluorine. We propose modifications to the fluorine mechanism to correct the discrepancies observed in the low pressure experiments, while simultaneously achieving good agreement with atmospheric pressure flame speed data in CH_4/air/CHF_3 flames, and, except in rich conditions ($\phi > 1.25$) CH_4/air/CH_2F_2 flames.

INTRODUCTION

The global ban on production of stratospheric ozone-depleting halons (bromine-containing fluorocarbons) has necessitated a search for alternative fire suppressants [1]. Hydrofluorocarbons (HFCs) are currently used in many instances where fire protection was previously provided by halons [2]. Since hydrofluorocarbons lack bromine, primarily responsible for both the fire suppression [3] and ozone depletion properties [1] of halons, HFCs must be employed in larger quantities to provide protection for an equivalent fire threat [4, 5]. Owing to space and weight limitations in many applications, HFC-based fire protection systems often must operate with smaller safety factors than halon systems. Safe and efficient use of HFCs thus requires greater understanding of their flame chemistry than was needed for the bromine based fire suppressants.

Recently, a chemical kinetic mechanism has been developed at the National Institute of Standards and Technology (NIST) to describe the relevant flame chemistry of C_1 and C_2 HFCs [6–9]. Studies of HFC kinetics are relatively sparse in comparison to the analogous hydrocarbon reactions, especially in view of the large (≈600 reactions involving fluorine species) reaction set. Therefore, kinetic mechanism development has had to rely extensively on computational modeling of reaction dynamics, and on analogies with equivalent hydrocarbon reactions [7]. The mechanism has been used to predict the behavior of hydrofluorocarbon inhibited flames in a variety of laboratory scale experiments [7, 10–13] with the eventual goal of modeling suppression of larger scale fires.

Comparison of model predictions with experimental data is necessary to validate and refine the current understanding of HFC combustion chemistry. To date, the effect of HFCs on

†National Research Council Postdoctoral Associate 1995–97. Present address: Dept. of Physical Sciences, New Mexico Highlands University, Las Vegas, NM 87701-4073.
*Corresponding author. E-mail: brad@code6185.nrl. navy.mil

COMBUSTION AND FLAME 117:709–731 (1999)

Published by Elsevier Science Inc.

0010-2180/99/$–see front matter
PII S0010-2180(98)00126-6

flames has been investigated primarily by measuring global parameters such as burning velocity, HF and CF_2O production, extinction strain rate, and flame temperature [11–18]. The detailed kinetics of hydrofluorocarbons in combustion environments, by contrast, has not been subject to extensive experimental investigation. There have been two studies that have reported species profiles in fluorocarbon inhibited flames by mass spectrometry [19, 20]. Vandooren et al. [19] compared several species in a $CO/H_2/O_2/Ar$ flame inhibited by CHF_3 to those in an inhibited flame and one inhibited by CF_3Br. The profiles of the stable hydrocarbon species as well as the radical species H, O, and OH, and the fluorinated species CHF_3, HF, and CF_2O were reported. Kinetic modeling was not performed; however, the authors concluded that the reactions

$$CHF_3 + H \Leftrightarrow CF_3 + H_2 \qquad (R1)$$

$$CF_3 + OH \Leftrightarrow CF_2O + HF \qquad (R2)$$

are primarily responsible for the reduction in concentration of the radicals H, O, and OH. It was also observed that CF_2O was a relatively stable product under the flame conditions used. Since the fluorine/hydrogen ratio was 1.5, the authors concluded that the low concentration of atomic hydrogen present in their flame was responsible for the persistence of carbonyl fluoride.

Sanogo et al. [20] studied a 31.5 torr (4.2 kPa) stoichiometric $CH_4/O_2/Ar$ flame inhibited with 1% C_2F_6. Profiles were recorded for several fluorinated species, including the radical species CF_3 and CF_2. Kinetic modeling was performed, using a different reaction set than the NIST mechanism. Agreement between the model and experiment was good for most species, but poor for CF_2 and CF_3, possibly due to the necessity of using a low electron impact energy in the mass spectrometer to avoid ion fragmentation [20].

Previous modeling studies have predicted the reaction pathways of fluoromethanes in low pressure flames [7]. Fluoromethanes are thought to react in flames through hydrogen atom abstraction by either OH radical or H atom attack. Since CF_4 does not have this pathway available to it, it is nearly inert in most flame environments [7]. The fluoromethyl radicals CF_3, CHF_2, and CH_2F produced, respectively, from CHF_3, CH_2F_2, and CH_3F, can react with H atoms, causing removal of either an H or an F atom to produce the methylene radicals $^1CH_2$, CHF, and CF_2.

Alternately, the CH_iF_{3-i} radicals can react with O or OH to form the carbonyl compounds CH_2O, CHFO, and CF_2O. CF_2O, carbonyl fluoride, is of particular interest because it is a relatively stable compound and is the only fluorine product besides HF likely to exit the combustion zone [7]. The kinetics of the CF_2O removal reactions assumed by the NIST mechanism, by reactions with H atoms and H_2O [5], have not been thoroughly characterized experimentally.

Here we present experimental data on intermediate species profiles in 10 torr methane/oxygen flames containing the series of fluoromethanes. It should be noted in making comparisons between experimental data and modeling predictions that the model was constructed primarily for use at atmospheric pressure [8], and most fluorocarbon association reactions included in the NIST mechanism are assumed to be in the high pressure limit. Intermediate species profiles in premixed flames are one of the best ways of verifying proposed kinetic pathways in a chemical mechanism but are only practical at reduced pressures. The situation is thus not ideal in that these experimental tests of the mechanism can only be performed outside its stated range of applicability. Nevertheless, many important features of the kinetic pathways (for instance, branching ratios of bimolecular reactions) should *not* be pressure dependent.

Because much of the development of the HFC kinetic mechanism has relied on analogies with the much better understood hydrocarbon flame chemistry, comparisons between molecules with differing degrees of fluorine substitution are a good way to investigate the fluorine kinetics. We therefore study a complete series of fluoromethanes. CHF_3 and CF_4 are used as fire suppressants, while CH_2F_2 is being considered as a replacement for chlorofluorocarbons in refrigeration applications [21]. CF_4 is thought to be inert in most flame environments because its only possible reaction pathway is the removal of a fluorine atom either by thermal dissociation

TABLE 1

Flame conditions used in experiment*

Agent	Flow rates (cm^3/min @ 0°C) CH_4	O_2	Agent	Adiabatic flame temperature (K)[a]	ϕ	Mass flow (g/cm^2-s)
none	400	800	0	2571	1.00	0.86×10^{-3}
CH_3F	167	800	350	2572	1.07	1.08×10^{-3}
CH_2F_2	342	800	175	2557	1.07	1.08×10^{-3}
CHF_3	400	800	117	2548	1.07	1.08×10^{-3}
CF_4	400	800	88	2538 (CF_4 inert)[b] 2541 (CF_4 reactive)[c]	1.00	1.07×10^{-3}

* The CHF_3, CH_2F_2, and CH_3F flames contain equal amounts of H, F, C, and O. The mass flow of CF_4 was chosen such that the F flux was equivalent to the other fluorine containing flames. All flames were operated at 10 ± 0.05 torr. The uncertainty of the flows is ±1% of the flow.

[a] Thermal equilibrium calculation [Gordon, S. and McBride, B., NASA Lewis Report NASA SP-273 (1976)].

[b] CF_4 only fluorine product considered in equilibrium calculation.

[c] Equilibrium distribution of fluorine products (predominantly HF).

or by abstraction, both of which have exceedingly slow kinetics [22]. Comparison of the CF_4 inhibited flame with other fluoromethane inhibited flames highlights the changes to the flame structure resulting from chemical activity as opposed to physical effects (oxygen dilution and increased heat capacity) of the agent [14].

The fluorinated intermediates CF, CF_2, CHF, and CF_2O were monitored by laser-induced fluorescence (LIF), as were the species H, OH, and CH. The profiles and relative concentrations of these intermediates can be used to infer the reaction pathways followed by the different fluorocarbons, along with their effect on the overall structure of the methane flame. Comparison of experimental radical profiles and kinetic modeling calculations in premixed flames can provide a more definitive indication of areas of kinetic mechanisms which need revision than can global parameters such as flame speed or extinction conditions.

EXPERIMENTAL

Flame Conditions

Table 1 shows the gas flow conditions of the five flames studied in this experiment. The following gases were used as received from the suppliers: CH_4, Air Products, 99.99%; O_2, MG Industries, 99.9%; Ar, MG Industries, 99.9%; CH_3F, PCR, 98%; CH_2F_2, PCR, 98%; CHF_3, Dupont, 99.9%; and CF_4, Air Products, 99.97%. The uninhibited flame was a stoichiometric methane/oxygen flame without any diluent gas. The four other flames each contained one of the compounds CH_3F, CH_2F_2, CHF_3, and CF_4. The mole fraction of CHF_3 added to the methane/oxygen mixture was about one third of the amount needed to blow the flame off the burner under the flow and pressure conditions used in our experiment. The relative amounts of the fluoromethanes were chosen such that all four inhibited flames contained equal numbers of fluorine atoms. The flow rates of methane and oxygen in the CHF_3 and CF_4 inhibited flames were the same as in the uninhibited flame. For the flames containing CH_3F and CH_2F_2, the methane flow rate was reduced to maintain the same equivalence ratio and concentrations of fluorine, carbon, and hydrogen as the flame containing CHF_3. These three flames (CH_3F, CH_2F_2, and CHF_3) are predicted to produce nearly identical concentrations of all final products, and the heat releases are nearly the same. The equivalence ratios for all the flames with added agent were slightly fuel rich ($\phi = 1.07$) with the exception of the flame containing CF_4, which had an equivalence ratio of unity.

The premixed flames were stabilized on a water-cooled burner (McKenna Products) enclosed in a vacuum chamber [23]. Flows were controlled using mass flow controllers (Sierra Instruments), with an accuracy of 1% of full scale. The premixed fuel, oxygen, and fluorocarbons flowed through a 6 cm diameter sintered

TABLE 2

Optical Diagnostics Used for Detection of Flame Species

Species	Transition	Excitation wavelength (nm)	Excitation energy (μJ)	Emission wavelength (nm)
H	1s-2s-4p (3 photon)	243.1 (2-photon) +486.1	150 10	486
OH	$R_1(8)$ A-X (1,0)	281.27	30	311
CH	$Q_1(6)$ B-X (0,0)	389.98	200	390
CF	$Q_2(21.5) + P_1(26.5) + Q_1(19.5)$ A-X (1,0)	223.30	200	255 ± 15
CF_2	$\tilde{A}$-$\tilde{X}$	250	60	334 ± 20
CHF	$\tilde{A}$-$\tilde{X}$ (0,3,0)-(0,0,0)	492.42	300	>515 nm
CF_2O	$\pi^*\leftarrow$n	211	80	320–400

stainless steel plate in the central portion of the burner. A concentric shroud flow was provided by flowing argon through a sintered brass ring that surrounded the burner, giving a mass flux per unit area at the burner surface equal to that of the flame reactants. The pressure inside the vacuum chamber was maintained at 10.00 ± 0.05 torr. The flame exhaust was passed through a soda-lime filter, then through a dry ice trap to remove water and hydrogen fluoride before entering the vacuum pump. Temperature and fluorescence profiles were recorded by translating the burner vertically inside the chamber using a stepper motor (Parker) while keeping the laser beam fixed.

OPTICAL DIAGNOSTICS

LIF diagnostics for the monitored species are summarized in Table 2. The detection schemes for the flame species have been discussed in greater detail elsewhere [24, 25]. Details relevant to individual molecules are noted in the results section. The fluorescence excitation source was a XeCl excimer-pumped dye laser (Lambda Physik EMG101E, FL2002). Excitation wavelengths below 300 nm were provided by frequency doubling the dye laser output using a BBO (β-BaB_2O_4) crystal. The probe beam entered the chamber parallel to the burner surface. The spatial resolution of the LIF profiles was limited by the 0.5 mm diameter of the unfocused probe beam. All windows on the chamber were made of either MgF_2 or CaF_2 to avoid chemical attack from HF.

Fluorescence was collected at right angles to the laser beam using a two lens collection system, which imaged a 0.25–1 cm section of the probe volume near the center of the burner. Filters were used to isolate the spectral region of interest, and the fluorescence was detected by a photomultiplier (Hamamatsu R1477). Resolved emission from the inhibited flames was characterized by replacing the emission filters with a 0.5 m monochromator (Jarrell-Ash).

The fluorescence signal was analyzed by a boxcar integrator, with a short gate (25 ns) set to the peak of the fluorescence decay. Where laser scatter interfered with the fluorescence signal, the boxcar gate was delayed some 30 ns from the peak PMT signal. Collision-induced quenching is minimized by these experimental protocols but is not removed entirely. Since the primary objective in the present study is to make relative measurements of species mole fraction between different inhibited flames, quenching only affects the overall result if the quenching environment is appreciably different between the various flames, or changes dramatically with location in a particular flame. The quenching environment should be similar for the flames studied, since they have similar concentrations of most major flame species. The quenching rates of the fluorinated radical species monitored in this study have not been extensively investigated. CF, CF_2, and CF_2O all have fluorescence lifetimes (radiative + predissociation) of 60 ns or less, so quenching should have little effect on the fluorescence signals of these species.

Changes in the excitation energy were moni-

tored by reflecting some of the incident excitation beam into a reference photodiode (UDT UV-100). The relationship between signal intensity and reference intensity was determined by attenuating the excitation beam with a series of neutral density filters. Most optical transitions were found to be slightly saturated. LIF profiles were obtained by correcting the measured LIF signal for changes in the excitation intensity. We have converted the LIF profiles to mole fraction profiles by correcting for gas density changes and the temperature dependence of the ro-vibronic level probed, except as noted below. We estimate the experimental uncertainties in the ratios of LIF signals between different flames to be ±10%.

Flame temperatures were determined by measuring rotational energy distributions of the OH radical by exciting the A-X (1,0) band near 281 nm. For the temperature measurements, the laser energy was attenuated to ≈2 μJ to avoid saturation. A broadband UV Filter (Corning 7-54) was used to collect fluorescence on both the (1,1) and (0,0) transitions. Spectral scans comprising typically between 10–40 spectral lines covering a broad range of rotational energies were performed at 15 points in each of the flame conditions used. Statistical uncertainties in the temperature fits ranged from 20–45 K. Burner surface temperatures were measured by an uncoated type K (Chromel-Alumel) thermocouple. For use in the premix calculations and in the conversion of the LIF data to species mole fractions, a temperature profile of the form

$$T(x) = \frac{A}{1 + B \exp\left(\dfrac{-(x - C)}{D}\right)} - Ex \qquad (1)$$

was used, where x is the height above the burner in cm. The coefficients A–E were determined by fitting the function to the experimental data points. These fitted functions were used as specified temperature inputs to the flame structure calculations discussed below.

MODELING

The chemical structures of the inhibited flames were modeled using the Sandia PREMIX and related codes [26–28]. The kinetic mechanism and thermodynamic database used for the H/C/O chemistry for one-carbon and two-carbon species was the Gas Research Institute GRI-Mech 2.11 [29], with nitrogen chemistry deleted. The NIST HFC mechanism is used for the thermodynamics and reactions of the fluorinated species [6–9]. The NIST mechanism has received some updates from that given in ref. [8]; the changes are listed in Table 3. This mechanism is referred to below as the base mechanism. Further adjustments to the mechanism were performed as discussed below.

The NIST mechanism includes nearly all one- and two-carbon species containing hydrogen, fluorine, and oxygen. The total reaction set includes 81 species and 759 reactions. Calculations of the experimental burner-stabilized flames were performed using the experimental temperature profiles as input. Multicomponent viscosities were used for species transport, and thermal effects on diffusivities were considered for the species H and H_2. The computational domain extended from the burner surface to 5 cm. Catalytic recombination of atomic hydrogen on the burner surface was not considered in the calculation. In both the experimental and calculated profiles, the H atom concentration is greatly reduced near the burner in the inhibited flames relative to the uninhibited methane/oxygen flame. Therefore the influence of burner surface chemistry on the structure of the inhibited flames will be less than on the uninhibited flame, where it has been found to have a rather minor influence [30]. Mesh refinement tolerances (local/global variation) for the species profiles were set to 0.1 for the species concentrations (the GRAD parameter in the PREMIX code) and to 0.25 for the concentration gradients (CURV parameter). The final grids for the uninhibited and CF_4 inhibited flames contained approximately 80 mesh points, while the solutions for the other three inhibited flames contained approximately 110 mesh points.

RESULTS

Temperature Profiles

Figure 1 shows the measured temperatures and the fitted functions. The flame containing CF_4

TABLE 3

Changes in Base Fluorine Mechanism From That Given in [8]

Reaction added:		Arrhenius parameters $k = AT^b \exp(-E_a/RT)$ A (cm, mol, s)	b	E_a (cal/mol)
1.	CH3OH + CH2F = CH3O + CH3F	1.44E+01	3.1	9800.
2.	CH3OH + CHF2 = CH30 + CH2F2	1.44E+01	3.1	9000.
3.	CH3OH + CF3 = CH3O + CHF3	1.44E+01	3.1	5500.
4.	CH3OH + CH2F = CH2OH + CH3F	3.20E+01	3.2	10,000.
5.	CH3OH + CHF2 = CH2OH + CH2F2	3.20E+01	3.2	9300.
6.	CH3OH + CF3 = CH2OH + CHF3	3.20E+01	3.2	5700.
7.	CF + CH2O = >CHF + HCO	1.00E+13	0.0	8000.
8.	CF + HCO = >CHF + CO	1.00E+13	0.0	0.
9.	CF:O + CF:O = CO + CF2:O	2.23E+13	0.0	318.
10.	CH3 − CHF + CH2O = CH3 − CH2F + HCO	5.50E+03	2.8	5900.
11.	CH3 − CF2 + CH2O = CH3 − CHF2 + HCO	5.50E+03	2.8	5900.
12.	CH2F − CH2 + CH2O = CH3 − CH2F + HCO	5.50E+03	2.8	5900.
13.	CH2F − CHF + CH2O = CH2F − CH2F + HCO	5.50E+03	2.8	5900.
14.	CH2F − CF2 + CH2O = CH2F − CHF2 + HCO	5.50E+03	2.8	5900.
15.	CHF2 − CH2 + CH2O = CH3 − CHF2 + HCO	5.50E+03	2.8	5900.
16.	CHF2 − CHF + CH2O = CH2F − CHF2 + HCO	5.50E+03	2.8	5900.
17.	CHF2 − CF2 + CH2O = CHF2 − CHF2 + HCO	5.50E+03	2.8	5900.
18.	CF3 − CH2 + CH2O = CH3 − CF3 + HCO	5.50E+03	2.8	5900.
19.	CF3 − CHF + CH2O = CH2F − CF3 + HCO	5.50E+03	2.8	5900.
20.	CF3 − CF2 + CH2O = CHF2 − CF3 + HCO	5.50E+03	2.8	5900.
21.	HCCO + F = CHF + CO	3.00E+13	0.0	0.
22.	CFCO + F = CF2 + CO	3.00E+13	0.0	0.
23.	C2H3 + F = C2H2 + HF	2.00E+13	0.0	0.
24.	CHF:CF[Z] + F = CHF + CF2	1.00E+13	0.0	0.
25.	CF2:CF + F = CF2 + CF2	2.00E+13	0.0	0.
Reaction numbers below refer to [8].				
Deleted:				
PP28.	CFO + O2 = CO2 + O + F			
New parameters:				
MA32.	HCO + CH2F = CH2CO + HF	3.00E+13	0.0	0.
MA33.	HCO + CHF2 = CHFCO + HF	3.00E+13	0.0	0.
MA34.	HCO + CF3 = CF2CO + HF	3.00E+13	0.0	0.
PP10.	CF3O + HCO = >CF2:O + HF + CO	5.00E+12	0.0	2000.
NN20.	CHF + O = CO + HF	9.00E+13	0.0	0.
NN42.	CF + OH = CO + HF	3.00E+13	0.0	1000.
GG50.	CH3 − CF2 + OH = CH2:CF2 + H2O	6.60E+13	0.0	3000.
GG67.	CH2F − CHF + HO2 = CHF:CHF[Z] + H2O2	4.00E+11	0.0	0.

had nearly the same temperature profile as the uninhibited flame; the flames containing the other fluoromethanes all had higher peak temperatures (attained slightly further above the burner surface) than the uninhibited flame, with the mono- and di-fluoromethane having slightly higher peak temperatures than the trifluoromethane flame. The temperature rise in the flames containing CF_4, CHF_3, and CH_2F_2 appeared to be pushed slightly (≈0.5 mm) further away from the burner surface, although the size of this effect was of the same magnitude as the uncertainty in the burner position (0.2 mm reproducibility uncertainty and 0.5 mm beam diameter).

Flame Emission Profiles

The uninhibited flame becomes noticeably brighter upon addition of CHF_3, CH_2F_2, or CH_3F. In the uninhibited flame, all of the structured emission in the 300–600 nm spectral region is due to OH*, CH*, and C_2^* [31]. No

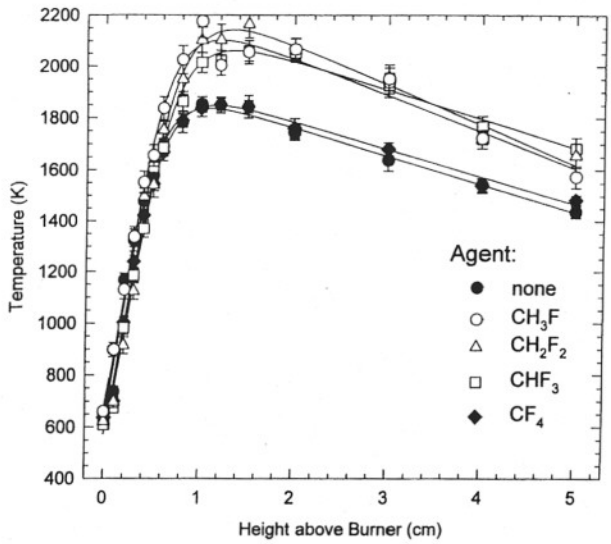

Fig. 1. Temperature profiles of the flames studied. Individual data points were determined from LIF spectra of OH; statistical uncertainties are shown. Solid lines indicate functional fits (see text), which were used as inputs to PREMIX calculations and in converting LIF profiles into relative mole fractions.

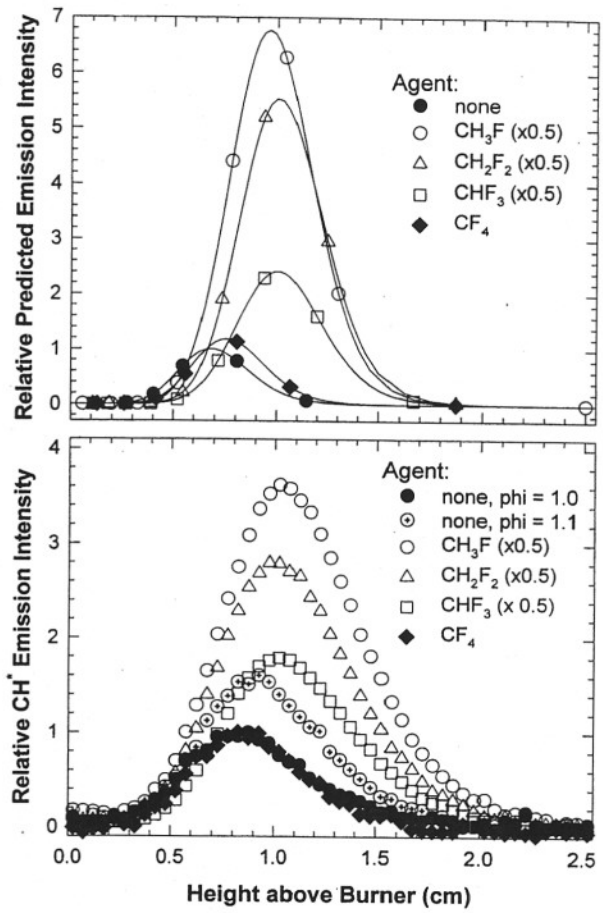

Fig. 2. CH* emission profiles (bottom) at 430 ± 10 nm for the uninhibited flame under standard flow conditions (equivalence ratio of 1.0), an uninhibited flame with an equivalence ratio of 1.1, and the flames inhibited by fluoromethanes. Profile for the flames containing CH_3F, CH_2F_2, and CHF_3 have been reduced by a factor of two. Emission profiles (top) estimated from the PREMIX calculation using the revised mechanism by taking the product of the O atom and C_2H concentrations.

additional spectral features appear upon addition of CHF_3, but the existing band systems increase in intensity by a factor of 1.25 in the case of OH*, and by a factor of approximately 3–4 for both CH* and C_2^*. The bottom panel of Fig. 2 shows CH* emission profiles at 430 nm for the uninhibited flame, the flames inhibited by the fluoromethanes, and an uninhibited flame with an equivalence ratio of 1.1, slightly greater than that of the inhibited flames. The flames containing CH_3F, CH_2F_2, and CHF_3 are all more than twice as luminous as the $\phi = 1.1$ flame, indicating that increased emission in the inhibited flames is not primarily an effect of richer stoichiometry. The luminous zone in these three flames moves approximately 2 mm further from the burner than its location in the uninhibited flame. The flame containing CH_3F produced the most CH* luminescence, followed by the CH_2F_2 flame, and then the CHF_3 flame. CF_4, in contrast, produces little change in the CH* emission profile.

Recently, the reaction

$$C_2H + O \Leftrightarrow CH^* + CO \qquad (R3)$$

has been identified as the primary source of CH* chemiluminescence in hydrocarbon flames [32]. Assuming a similar quenching environment for the different flames, the CH* emission profile can be expressed as

$$I_{CH^*} = k_{R3}(T)[C_2H][O]. \qquad (2)$$

The overall reaction $C_2H + O \rightarrow$ products is written in the GRI mechanism as being temperature independent. The rate of the CH* channel has only been measured at room temperature [32]. If we assume that the branching ratio is temperature independent, the CH* emission intensity is then given by the product of the C_2H and O atom concentration profiles. The product of the calculated profiles for the various flame conditions is plotted in the top panel of Fig. 2.

The predicted O atom concentrations in the various flames vary by less than a factor of two, so the CH* emission intensity will be governed chiefly by the C_2H profile. The formation of C_2 species in the flames containing fluoromethanes is predicted to be dominated by methyl + fluoromethyl recombination reactions:

$$CH_3 + CH_iF_{3-i} \rightarrow CH_2{=}CH_iF_{2-i} + HF. \quad \text{(R4)}$$

The CH* emission profiles give an indication (albeit an indirect one) of the importance of the C_2 chemistry in the inhibited flames. Evidently the recombination of fluorinated methyl radicals with CH_3 is more facile than the recombination of two methyl radicals.

Intermediate Species Profiles

H

Calculated and measured H profiles are shown in Fig. 3. Hydrogen atoms were detected by a two-step excitation process involving a two photon absorption at 243 nm (150 μJ focused with a 35 cm focal length lens) from the 1s to 2s state, followed by a single photon excitation at 486 nm (5–10 μJ, unfocused) to the 4p state [33, 34]. Fluorescence was detected at 486 nm. The intensity of the 486 nm beam was adjusted to be near the saturation intensity, while the LIF signal exhibited a quadratic dependence on the 243 nm laser energy. Interference presumably from CF_2 was noted in the flames inhibited by CH_2F_2 and CHF_3; the interference signal depended only on the presence of the 243 nm light. There was also a small amount of laser scatter at 486 nm. To correct for these complications, the fluorescence signal was recorded with each of the two beams blocked, and these profiles were subtracted off the profile recorded with both beams present.

The peak H mole fractions in all the flames are nearly identical, although the CHF_3, CH_2F_2, and CH_3F inhibited flames have higher peak temperatures, which would normally tend to increase the radical's mole fraction. The position of the H concentration rise in the CHF_3, CH_2F_2, and CH_3F inhibited flames is moved further away from the burner.

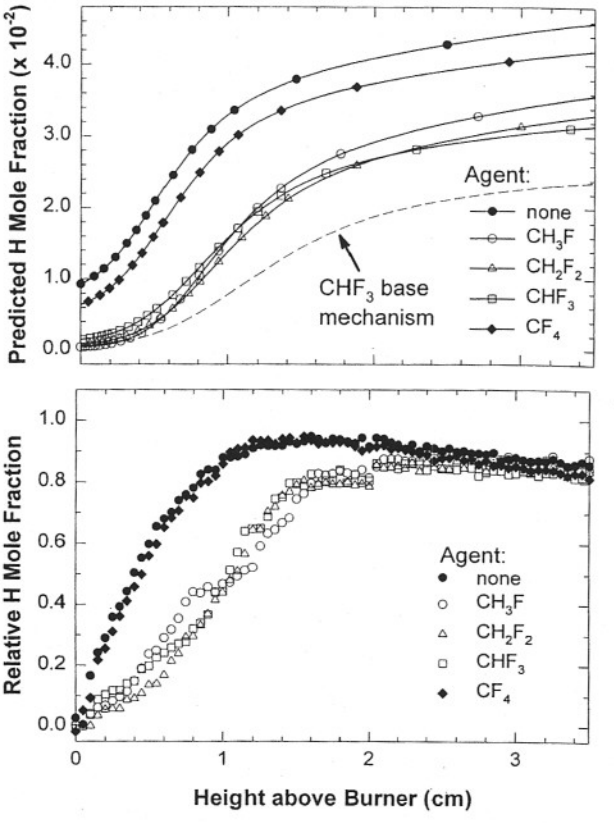

Fig. 3. Calculated (top) and measured (bottom) H atom profiles. Predictions using the revised mechanism ([8] plus Tables 3 and 4) are indicated by solid lines, the prediction using the base mechanism ([8] plus Table 3) for the CHF_3 flame is shown in dashed lines. Predictions for the other inhibited flames using the base mechanism were similar to those using the modified mechanism.

OH

Calculated and measured OH profiles are shown in Fig. 4. LIF profiles of the hydroxyl radical were recorded by exciting the $R_1(8)$ line of the A-X (1,0) band. Fluorescence was detected both on the (1,1) and (0,0) bands [35]. Typical laser energies were 30 μJ for recording profiles. For temperature measurements, the probe energy was attenuated to 2 μJ in an unfocused beam of approximately 0.01 cm^2 cross section to avoid saturation of the transition.

The OH profiles have many features in common with the H atom profiles, which is to be expected given the fast equilibrium between the two species [36]. As with the H atoms, the OH profiles are almost identical for the uninhibited and the CF_4 inhibited flames. The peak OH mole fractions of the CHF_3, CH_2F_2, and CH_3F inhibited flames were similar to that of the unin-

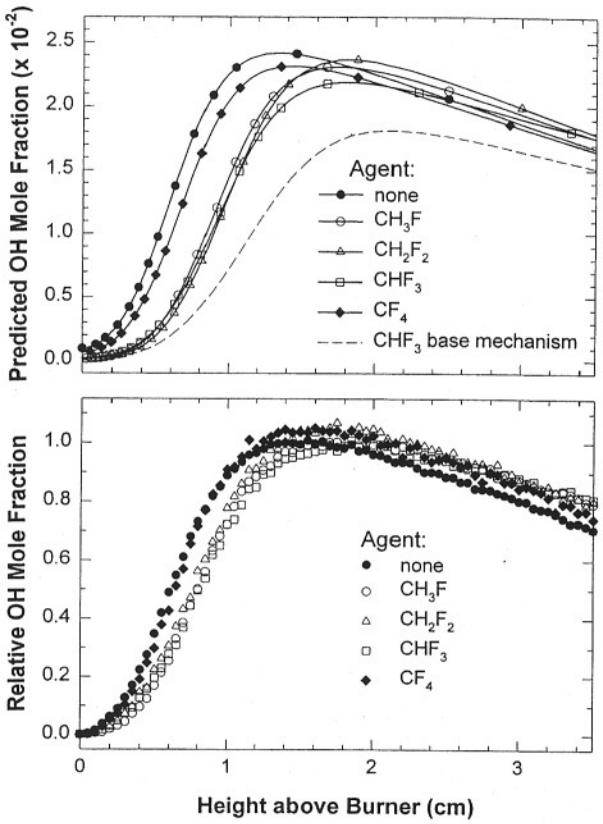

Fig. 4. Calculated (top) and measured (bottom) OH profiles. Predictions using the revised mechanism are indicated by solid lines, the prediction using the base mechanism for the CHF_3 flame is shown in dashed lines. Predictions for the other inhibited flames using the base mechanism were similar to those using the modified mechanism.

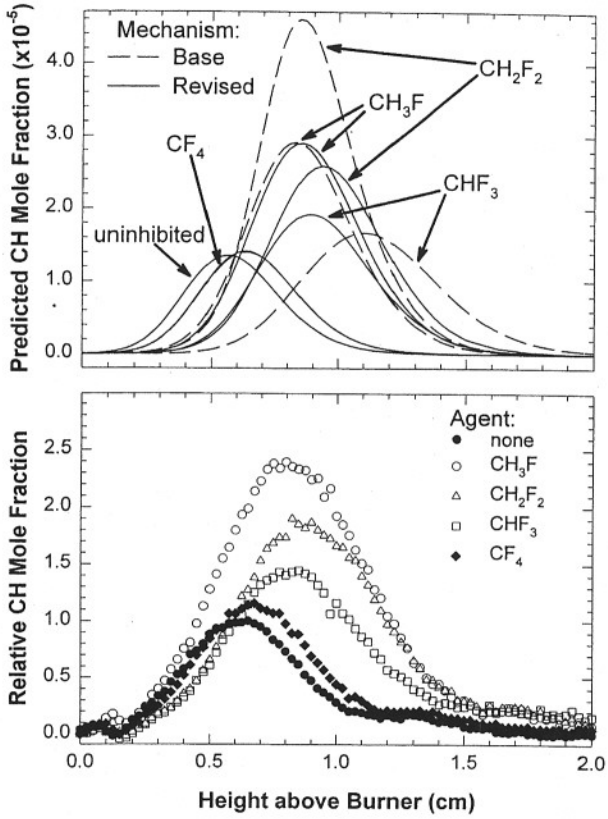

Fig. 5. Calculated (top) and measured (bottom) CH profiles. Calculations using the revised mechanism are shown in solid lines, those using the base mechanism are shown in dashed lines. For the CF_4 inhibited flame, the two calculations are indistinguishable.

hibited flame, but as with the H atom profiles, the OH concentration rise occurred further from the burner than predicted by the model.

CH

Calculated and measured CH profiles are shown in Fig. 5. The CH radical was monitored on the $Q_1(6)$ line of the B-X (0,0) band near 390 nm [37]. Fluorescence was monitored at the same wavelength. Typical pulse energies were 200 μJ in an unfocused beam. Due to scattered laser light, the boxcar gate was delayed by 30 ns relative to the laser pulse.

The profiles of ground state CH show much less sensitivity to the addition of the agents than do the profiles of CH* emission. The peak CH mole fraction is increased in all of the inhibited flames; the effect is greatest in the flame inhibited by methyl fluoride, in which the peak CH mole fraction increases by some 70%. The CH mole fraction profile is slightly increased (by about 10%) in the flame inhibited by CF_4.

CF_2

Calculated and measured CF_2 profiles are shown in Fig. 6. The CF_2 radical was detected by exciting at a wavelength of 250 nm, roughly in the middle of the $\tilde{A}$-$\tilde{X}$ transition, which at room temperature extends from 270 to 220 nm [25]. Typical pulse energies were 60 μJ, unfocused. Fluorescence was collected at 334 nm, using a 20 nm bandpass filter. The fluorescence signal was extremely strong, and the light had to be attenuated so that the PMT could operate in a region of linear response.

The flame excitation spectrum of CF_2 is essentially a continuum due to substantial populations in numerous excited ro-vibrational levels at combustion temperatures. Since the rotational transition(s) probed are unknown, we

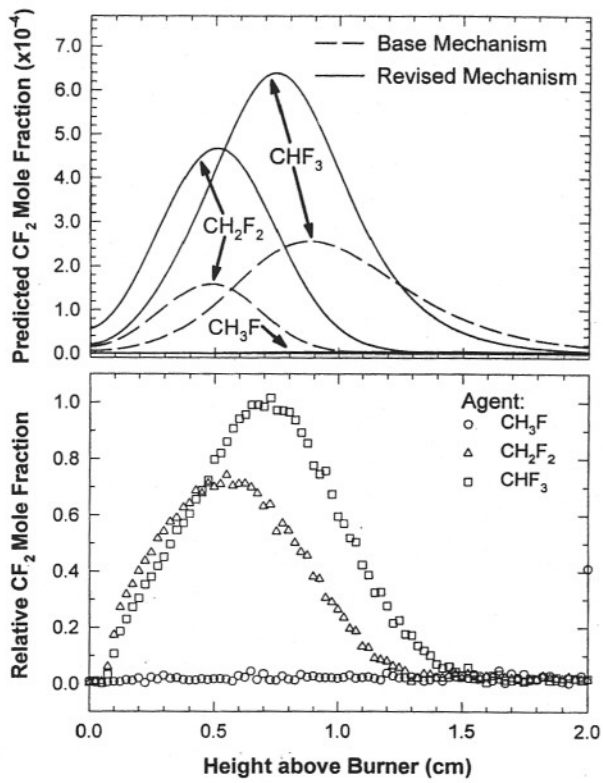

Fig. 6. Calculated (top) and measured (bottom) CF_2 profiles. Calculations using the revised mechanism are shown in solid lines, those using the base mechanism are shown in dashed lines. No CF_2 fluoresence signal was detected in flames inhibited by CF_4 or CH_3F.

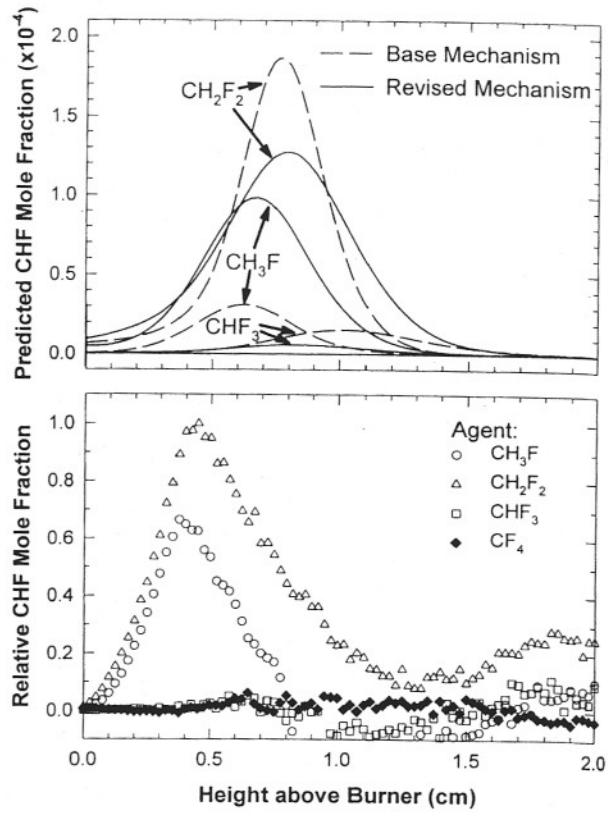

Fig. 7. Calculated (top) and measured (bottom) profiles of CHF. Calculations using the revised mechanism are shown in solid lines, those using the base mechanism are shown in dashed lines. Fluorescence signal from CHF is not observed in the flame containing CF_4. Near 1.0 cm the profiles may have been affected by saturation of the detector due to flame emission (see text).

have corrected the LIF profiles only for density variations in the flame. The lack of distinct spectral features makes it difficult to prove that CF_2 is indeed the source of the LIF signal. The observed fluorescence decay time of ≈60 ns, however, matches the reported value for CF_2. Also, the signal is present in the flames containing CHF_3 and CH_2F_2, but not CH_3F, strongly suggesting that the source must have two fluorine atoms. The intense fluorescence from CF_2 interferes with the detection of other species such as CF, OH, H, and CF_2O. The structureless interference due to CF_2 may be easily subtracted off from profiles of OH, CF, and H atoms, which have well structured spectra. For larger molecules such as CF_2O, interference from CF_2 inherently limits the detection sensitivity.

CF_2 is slightly more abundant in the CHF_3 flame than in the CH_2F_2 flame. CF_2 appears later in the CHF_3 flame than in the CH_2F_2 flame, indicating that the reaction pathway $CHF_3 \Rightarrow CF_3 \Rightarrow CF_2$ occurs more slowly than the analogous pathway $CH_2F_2 \Rightarrow CHF_2 \Rightarrow CF_2$. The CF_2 concentrations in the CH_3F and CF_4 inhibited flames are less than 1% that of the CHF_3 flame. No CF_2 signal was observed in the CF_4 inhibited flame even when the CF_4 flow was quadrupled.

CHF

Calculated and measured profiles of CHF are shown in Fig. 7. CHF was excited on the most intense bandhead of the (0,3,0)–(0,0,0) band of the $\tilde{A}$-$\tilde{X}$ transition near 492 nm [25, 38]. CHF represents an intermediate case between the strongly fluorescent CF_2 molecule, and $^1CH_2$, which can only be detected in flames with extreme difficulty [39]. We chose the (0,3,0)–(0,0,0) band to attempt to detect CHF because it has a shorter radiative lifetime than the bands

at longer wavelengths and fluoresces in a region relatively free from interference [38]. A significant fluorescence signal from CHF is observed in the flames containing CH_3F and CH_2F_2 but not CHF_3 or CF_4. Since CHF_3 is thought to react predominantly by abstraction of the hydrogen atom, the observed pattern is consistent with the assignment of CHF as the source of the LIF signal and also the model's prediction of the reaction pathways of the fluoromethanes in flames.

A rotational analysis has not been carried out for this band, making it difficult to convert the LIF profiles into mole fractions. Unlike the CF_2 spectrum, the CHF spectrum displays appreciable structure, so temperature corrections to the spectrum are probably more significant. We have estimated the temperature influence on the LIF signal by assuming a ground state rotational energy of 300 cm^{-1}. The rotational energy of the spectral feature used for monitoring is unknown but is probably fairly low since room temperature spectra of CHF also display prominent band heads. The major influence on the temperature correction is the rapid increase in the molecular partition function due to population of higher rotational and vibrational states. The converted profiles are shown in the bottom panel of Fig. 7. The exact shape and peak location is only approximate due to the large and uncertain temperature correction. Furthermore, in the luminous zones of the flames (>8 mm above the burner), there was some saturation of the photomultiplier due to background luminescence, resulting in a baseline drift. Although the locations of the calculated peak CHF concentrations disagree by about 3 mm with the experimental values, this is not necessarily significant in light of the uncertainties in the data analysis. The data does indicate that CHF peaks slightly earlier and at a ≈30% lower mole fraction in the CH_3F flame than in the CH_2F_2 flame.

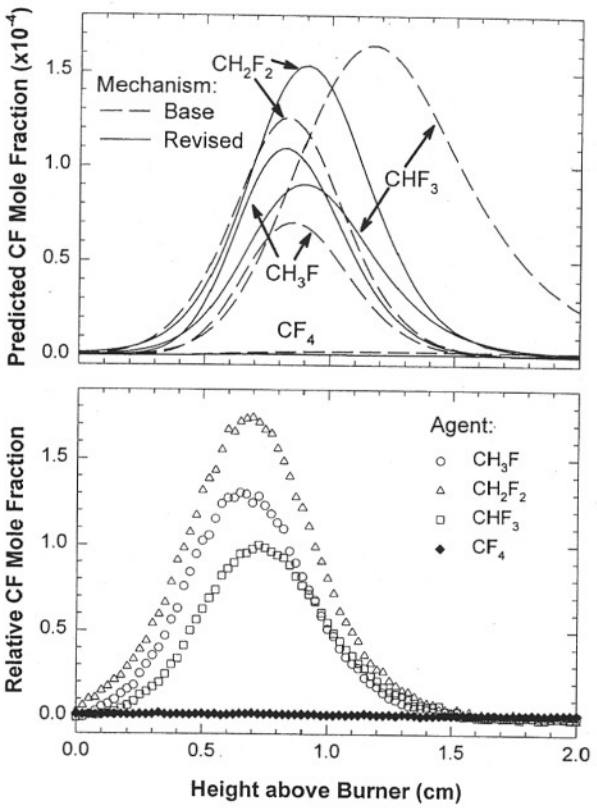

Fig. 8. Calculated (top) and measured (bottom) CF profiles. CF was produced in detectable amounts from all agents except CF_4. Calculations using the revised mechanism are shown in solid lines, those using the base mechanism are shown in dashed lines.

CF

Calculated and measured CF profiles are shown in Fig. 8. CF was excited on the overlapping resonance lines $Q_2(21.5)$, $P_1(26.5)$, and $Q_1(19.5)$ of the A-X (1,0) band at 223.299 nm [40]. Fluorescence was detected on the (1,4) and (1,5) bands [41] using a 15 nm bandpass filter centered at 255 nm. Typical pulse energies were 200 μJ in an unfocused beam. Since CF is one of the few fluorine species which has a well-defined spectrum at flame temperatures, interference from CF_2 was corrected for by tuning the laser just off the CF line and subtracting this background signal from the profiles. The fluorescence lifetime was approximately 20 ns, consistent with previous determinations [41]. There was essentially no scattered light transmitted by the filter, so the boxcar gate was set to the peak of the laser pulse. CF was produced in detectable amounts from all the agents except for CF_4.

CF_2O

Carbonyl fluoride is detectable by LIF but has a rather weak signal and a broad featureless spectrum at flame temperatures. We attempted to record profiles of CF_2O in the inhibited flames but were unsuccessful due to very weak signals,

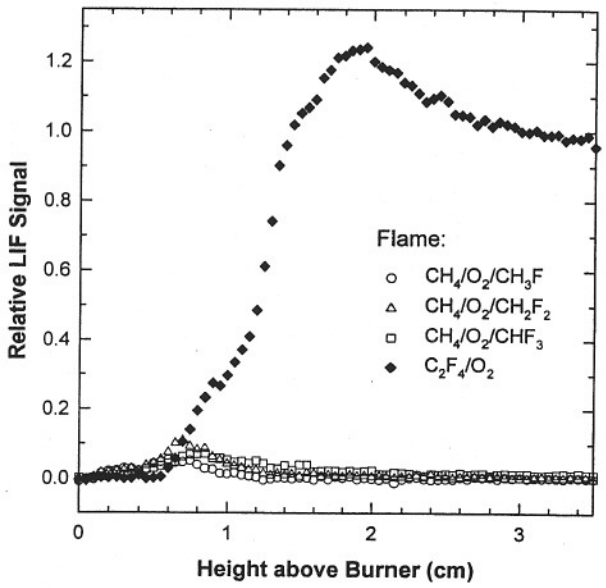

Fig. 9. LIF Profiles of CF_2O. A profile of CF_2O was obtained from a C_2F_4/O_2 flame [25, 42]. The signal obtained from fluoromethane inhibited CH_4/O_2 flames is many times weaker and may be complicated due to interference from CF_2 and vibrationally excited O_2.

as well as interference from other species, including CF_2 and vibrationally excited O_2. We were, however, able to set an upper bound on the amount of carbonyl fluoride which could be present in the inhibited flames, based on comparison with the C_2F_4/O_2 flame where CF_2O is a stable product and is produced in abundance [42]. Figure 9 shows profiles recorded at an excitation wavelength of 211.03 nm in the HFC inhibited CH_4/O_2 flames, as well as in a 20 torr C_2F_4/O_2 flame identical to the 35% fuel case of Douglass et al. [42]. The signal in the C_2F_4 flame is primarily due to CF_2O, especially in the region above 1.5 cm. Time-resolved fluorescence decays can distinguish fluorescence contributions from CF_2 and oxygen observed closer to the burner; the lifetime of CF_2 is 60 ns, the lifetime of O_2 is less than 15 ns (limited by the laser pulse width), while that of CF_2O is 30 ns [25].

The signal level in the inhibited methane flames is many times weaker than that of the C_2F_4/O_2 flame. In the C_2F_4/O_2 flame studied for comparison, the partial pressure of CF_2O at 20 torr is predicted to be 6 torr in the post-flame zone [42]. The LIF signal is at least 80 times weaker in the post-flame zone (x = 3.0 cm) of the inhibited methane/oxygen flames under the same excitation and detection conditions. This indicates that CF_2O has a mole fraction of less than 0.01 in the inhibited methane/oxygen flames; less than 10% of the F atoms in the flames studied exit the reaction zone as CF_2O. This upper bound to the CF_2O mole fraction is consistent with the prediction of the chemical kinetic mechanism for these flames. Evidently interferant species contribute to the fluorescence as an appreciable LIF signal is observed in the reaction zone in the uninhibited as well as the inhibited flames. It is not clear how much of the fluorescence is due to CF_2O.

Analysis and Mechanism Refinement

Calculations using the base mechanism are shown in dashed lines in Figs. 3–8. For the CHF_3 flame the predicted location of the reaction zone (as indicated by any of the intermediate species monitored here) is several mm too far from the burner. Furthermore, the relative concentrations of the intermediate species for the different agents are not always well predicted. The concentrations of the fluorinated intermediates CF and CF_2 are overpredicted in the trifluoromethane flame relative to the flames containing the other agents. CHF is underpredicted in the CH_3F flame relative to the CH_2F_2 flame. The CH mole fraction is overpredicted in the CH_2F_2 flame compared to all the other flames. CH* emission based on the product of the C_2H and O atom profiles is overpredicted in the CH_3F and CH_2F_2 flames.

To remedy these deficiencies, we carried out a sensitivity and reaction path analysis and adjusted selected rates of reactions involving fluorinated species in an iterative process. Our goal was to improve predictions of our low pressure data, while simultaneously achieving good agreement with published data on atmospheric pressure flame speeds for methane/air flames containing CHF_3 and CH_2F_2. In addition to constructing a better validated model, we also hoped to identify individual reactions which may require further experimental or theoretical investigation.

Recently, Saso et al. [12] have recommended adjustments to the reactions of CHF_3 and FCO with H, as well as FCO thermal decomposition,

to better fit the atmospheric pressure propagation speed of CHF_3 inhibited flames. Included in [12] was modeling of our preliminary data for CH, CF, CF_2, and OH in the uninhibited and CHF_3 inhibited flames. Even with the refinements, the model still predicted too great a standoff distance (distance from the burner surface to the maximum of the intermediate profiles) for our CHF_3 flame conditions.

To investigate the cause of this discrepancy, we calculated sensitivities of the burning velocity of low pressure freely propagating flames. In general, a higher adiabatic burning velocity in a freely propagating flame is equivalent to a reduced standoff in a burner stabilized flame, since the closer the flame front is to the burner, the greater the heat loss while still maintaining a (nonadiabatic) flame speed equal to the gas flow velocity. Thus, a predicted standoff which is too large generally means that the flame speed has been underpredicted. For all the fluoromethanes which contain hydrogen, a rate increase in the thermal decomposition of the agent to eliminate HF is predicted to increase the flame speed, while hydrogen abstraction by O, H, or OH nearly always has a negative sensitivity coefficient, meaning that an increase in the reaction rate decreases flame speed. In the HFC mechanism nearly all reactions are reversible, so an increase in the rate coefficient will increase both the forward *and* backward rates commensurately.

Thermal Decomposition Reactions

For the CHF_3 flame in particular, the reaction

$$CHF_3 \Leftrightarrow CF_2 + HF \qquad \text{(R5)}$$

had the second highest sensitivity coefficient, following the reaction of CHF_3 with OH, and ahead of the three reactions to which Saso et al. proposed modifications. Furthermore, in the base mechanism, the H and OH mole fractions are underpredicted in the CHF_3 flame relative to the uninhibited case; these profiles also were found to have high sensitivities to reaction (R5).

In refining the HFC mechanism, we have adopted the recommendations of Saso et al. Nevertheless, these adjustments yielded only a slight improvement in the predicted position of the reaction zone, similar to the finding in [12]. It appears that reaction (R5) is the culprit in the inaccurate prediction of the position of the intermediate profiles.

Since the thermal decomposition reactions of the fluoromethanes are important in predicting the flame speed and structure, it is necessary to consider their pressure dependence for our conditions. In the case of CHF_3, the reaction is written in the falloff regime in the base mechanism, following the study of Hidaka et al. [43]. The reactions of CH_3F and CH_2F_2, by contrast, are written as being unimolecular in the HFC mechanism. Although the prediction of the flame standoff distance for the base mechanism is reasonable for mono- and di-fluoromethane, the assumption of the decomposition reactions being pressure independent is unreasonable at 10 torr. The kinetics of the CH_3F decomposition reaction are based on the study of Schug and Wagner [44] (but written in the opposite direction), who derived both unimolecular and bimolecular kinetics parameters. We have used the parameters of [44], assuming a Lindemann falloff behavior. At atmospheric pressure, the reaction rate is in the low-pressure limit above about 1600K due to the reduction of the molecular density as temperature increases at a fixed pressure. At 10 torr, the reaction is in falloff over the entire temperature range of interest.

The decomposition kinetics of CH_2F_2 are based on a RRKM calculation performed for the HFC mechanism development. As with the CHF_3 and CH_3F decompositions, this rate is likely to also be in falloff at atmospheric pressure and below. Therefore, we have converted the kinetic parameters to a bimolecular rate while keeping the rate at atmospheric pressure unchanged. Several other decomposition pathways exist for the fluoromethanes, but the HF elimination channel is, according to sensitivity and reaction pathway analysis, by far the dominant route for the hydrofluoromethanes. We have not put in falloff behavior for the other channels, since they are unlikely to have a significant effect on the mechanism's overall performance.

We have added falloff behavior to all other decomposition reactions, which, according to the base mechanism, were predicted to be important for our conditions. The reactions $CF_4 \Leftrightarrow CF_3 + F$ and $CF_2 \Leftrightarrow CF + F$ were converted to bimolecular rates. For CF_4, the decomposition

reaction, along with F atom abstraction by H, is the only possible destruction mechanism. Sensitivity analysis showed that the CF_2 thermal decomposition reaction was predicted to have a significant influence on the propagation speed of the trifluoromethane flame, at least when it was written as being unimolecular. After being converted to a bimolecular rate, the influence of this reaction was greatly reduced. Also, the decomposition reactions of fluoroethylenes to eliminate HF were predicted to dominate destruction of $CF_2{=}CH_2$ and $CHF{=}CH_2$, which are formed in the CHF_3 and CH_2F_2 flames, respectively, by the reactions:

$$CF_3 + CH_3 \rightarrow CH_2{=}CH_2 + HF, \qquad \text{(R6)}$$

$$CHF_2 + CH_3 \rightarrow CHF{=}CH_2 + HF. \qquad \text{(R7)}$$

Reactions (R6) and (R7) are predicted to be the dominant route to formation of C_2 species under our conditions. The thermal decomposition of the resulting fluoroethylenes has only been investigated above 4 atmospheres, where it appears to be in the high pressure limit [45, 46]. We have added falloff behavior to these reactions, assuming that the transition between high pressure and falloff occurs somewhere in the vicinity of atmospheric pressure.

Another issue is the third body efficiencies of flame species for these decomposition reactions. The NIST mechanism includes no third body efficiencies for the CHF_3 decomposition reaction; all the shock tube studies on CH_3F and CHF_3 decomposition [43, 44] were performed in argon. We have assumed third body efficiencies for these reactions equal for most species to those given in the GRI mechanism for methane dissociation, along with efficiencies of 2 for HF, 9 for water, and 6 for the fluoromethanes. The low pressure A factors in the decomposition reactions have been divided by 0.7 (the relative third body efficiency used in GRI-mech for Ar for most decomposition reactions). The net result is that the overall third body efficiency in the flame reaction zones is increased by a factor of six relative to argon. In methane/air flames, the effect is much less significant since N_2, which by definition is assigned a relative third body efficiency of unity, has a mole fraction of approximately 70% throughout the flame.

H_2 vs. HF Elimination in Chemically Activated Decompositions

Reaction pathway analysis indicates that the greatly overpredicted peak CH mole fraction in the CH_2F_2 flame is due to the reaction

$$CHF + H \Leftrightarrow CH + HF. \qquad \Delta H_f = -21 \text{ kJ} \qquad \text{(R8)}$$

The kinetic parameters for this reaction in the HFC mechanism are based on the study of Tsai and McFadden [47], which measured the total disappearance rate of CHF. The alternate channel,

$$CHF + H \Leftrightarrow CF + H_2, \qquad \Delta H_f = -92 \text{ kJ} \qquad \text{(R9)}$$

is lower in energy, but was not included in the HFC mechanism. Tsai and McFadden detected both CF and CH products but were unable to determine a branching ratio due to secondary reactions and uncertainties in detection efficiency. The lack of a significant increase in the CH concentration in the difluoromethane flame relative to the other inhibited flames indicates that the CF channel is the dominant one. We have put in a branching ratio of approximately 70% for Reaction (R9) while keeping the total rate of reactions (R8) and (R9) fixed to the measured value.

The reaction

$$HF + CH \rightarrow CF + H_2, \qquad \text{(R10)}$$

which according to the base mechanism was predicted to be quite important, is essentially equivalent to a redistribution of the branching ratio between reactions (R8) and (R9). The rate in the base mechanism was set to the upper limit suggested by RRKM calculations. Adding reaction (R9) to the mechanism allowed this rate to be lowered by one third to better match the peak CH concentrations in the flames inhibited by CH_3F, CH_2F_2, and CHF_3 relative to the uninhibited flame.

The product channels of the fluoromethyl reactions with atomic hydrogen

$$CH_iF_{3-i} + H \rightarrow CH_iF_{2-i} + HF \qquad \text{(R11)}$$

$$CH_iF_{3-i} + H \rightarrow CH_{i-1}F_{3-i} + H_2 \qquad \text{(R12)}$$

is another area of the mechanism to which the experimental data suggests some modifications. The base mechanism predicts that the HF channel overwhelmingly dominates (>96% branching ratio for both mono- and di-fluoromethyl radicals), largely on the basis of a lower energy barrier assuming the reaction proceeds through a chemically activated fluoromethane intermediate. The H_2 channel could also proceed via a direct abstraction as well as by elimination from a complex, whereas abstraction of a fluorine atom would occur at an extremely slow rate.

In the methyl fluoride flame, the base mechanism predicts that CH_2F radicals are nearly all converted to $^1CH_2$ by the reaction by atomic hydrogen. Very little CHF is predicted to be formed in this flame relative to the CH_2F_2 flame. Formation of CF in the CH_3F flame is predicted to occur almost exclusively via the CH + HF reaction. In the difluoromethane flame, formation of CF_2 is predicted to occur primarily through the disproportionation reaction with methyl radicals:

$$CHF_2 + CH_3 \rightarrow CF_2 + CH_4. \qquad \text{(R13)}$$

This reaction causes a slight overprediction of CF_2 in the CH_2F_2 flame relative to the CHF_3 flame when kinetics of the fluoromethane decomposition reactions are placed in the falloff regime.

The rate of (R13) has been reduced to correctly predict the ratio of CF_2 between the difluoromethane and trifluoromethane flames. The kinetics of the CHF_2 + H reactions have not been altered in our modification. It is conceivable that H atoms, rather than CH_3 radicals, constitute the primary reaction partner leading to CF_2 formation from CHF_2, although our data provide no information on this issue. One study [48] at room temperature reported that CF_2 and CHF were produced in comparable amounts from the H + CHF_2 reaction. For the CH_2F + H reaction, we have increased the branching ratio of the CHF + H_2 channel to better predict the CHF and CF profiles. In the reactions of CHF, CH_2F, and CHF_2 with H atoms, formation of H_2 is in all cases the lowest energy product channel, and it seems plausible that the branching ratios may be higher than the base mechanism predicts. Further investigation of the product channels of these reactions would be extremely useful.

Relative Importance of H, O, and OH Reaction Partners With Hydrofluorocarbon Radicals

The fluoromethyl and fluoromethylene radicals can react with atomic hydrogen as described above, or with O or OH to form the oxidized species CF_2O, CHFO, FCO, and HCO. In the base mechanism, reaction with H is predicted to be the dominant path in most cases. Since the O and OH reactions produce different products than the H reactions, the relative reaction rates with the different partners will influence the net yield of, for instance, CF from CF_2. These reactions will thus affect the profiles of the species we have detected, although unfortunately none of the oxygen containing products are sufficiently amenable to LIF diagnostics to obtain a direct measurement of their profiles. CHFO and HCO both have transitions in the vicinity of 250 nm, but interference from CF_2 would preclude their detection at these wavelengths for our conditions. Some kinetic studies have been performed on O atom reactions with the hydrofluorocarbon radicals, but the OH reaction rates have, in most cases, never been directly measured. In the HFC mechanism, the OH kinetics are largely based on the analogous O atom reactions.

Kinetic rates of the reactions of CF_2 with H and O atoms have been measured at room temperature by Tsai and McFadden [49, 50], while the reaction rate with OH has only been inferred from kinetics modeling of flames inhibited by CF_3Br performed by Biordi et al. [51, 52]. The base mechanism assumes that the reaction rates with O and particularly with H increase with temperature, the result being that at flame temperatures, CF_2 is almost quantitatively converted to CF by the reaction with H atoms. The base mechanism greatly overpredicts the amount of CF in the trifluoromethane flame relative to the mono- and di-fluoromethane flames. The only way to reasonably bring the predicted CF concentrations into agreement with the experiment is to assume that CF_2 has reaction rates with O and/or OH comparable to those with H under flame conditions. We have made the rates temperature independent and set the rate with OH to four times the value for O.

The rate of the reaction CHF_2 + OH → CHFO + HF was reduced by a factor of two to

better fit the CHF and CF profiles in the difluoromethane flame. The reaction CF + OH → CO + HF has been increased to move the CF concentration peak closer to the burner. Even in the revised mechanism, the CF profiles in all the flames remain about 2 mm too far from the burner, even though the H, OH, CH, and CF_2 profile maxima are all predicted to within 1 mm of the experimental value for all the flames. Since the reaction zone as a whole is predicted to occur in the right place, the problem seems to be that either the CF formation or removal kinetics are too slow. Since CF is produced primarily from CHF in the methyl fluoride flame (in the revised mechanism) and from CF_2 in the trifluoromethane flame, there is not a single CF formation reaction that can be responsible for the late CF peak in all three flames. Concerning the removal kinetics, the reaction rates of CF with H and O have been measured at room temperature only [49, 50, 53], while the rate with OH has not been measured. The recent measurement of Van Hoeymissen et al. [53] for the CF + O reaction measured a value three times larger than did the study of Tsai and McFadden [50], from which the kinetic parameters in the base mechanism have been taken. We have increased the rates by a factor of two at high temperatures for the H and O reactions while maintaining the same rates as in the base mechanism at 300K and increased the rate with OH. These changes moved the CF profile slightly toward the burner but not enough to obtain good agreement with the experimental profiles. It is also conceivable that the rate of CF + O_2 should be increased at high temperature, since O_2 is the most important reaction partner in CF removal. The preexponential factor assumed in the base mechanism, 2×10^{13} cm^3/mol-s, however, is already fairly high for a radical reaction with a closed shell species, and approaches that of the analogous reaction for CH, which is generally observed to be more reactive than CF [53].

The recombination rates of the fluoromethyl radicals CH_2F and CHF_2 with CH_3

$$CH_2F + CH_3 = C_2H_4 + HF, \qquad (R14)$$

$$CHF_2 + CH_3 = CHFCH_2 + HF \qquad (R15)$$

have been lowered by 30% from the base mechanism. The base mechanism predicts that the C_2H concentration (and by extension the amount of CH* emission) should be three times as high in the mono- and di-fluoromethane flames as in the trifluoromethane flame, whereas the experimental ratio of the CH* emission profiles is slightly less than a factor of 2. Sensitivity analysis for C_2H concentrations found that the reactions above had the highest sensitivities of any reactions involving fluorine because they constitute the principal route to formation of C_2 species in these flames. Even with the revisions, the ratio of predicted CH* emission is still too high. Further adjustment of the rates is probably not warranted based on the emission profiles. Both the temperature dependence of the $C_2H + O \rightarrow CH^*(A^2\Delta) + CO$ reaction and detailed validation of the C_2 hydrocarbon and fluorocarbon kinetics leading to C_2H formation require further investigation.

Reaction Pathways and Profile Comparisons With Experiment

Reaction pathways of the fluorinated agents in the burner stabilized flames were determined by integrating the chemical production rates across the flame zone and summing individual rates with all possible reaction partners. The results for the base mechanism are shown in Figs. 10, 12, and 14, for the flames containing CH_3F, CH_2F_2, and CHF_3, respectively. Predictions for the revised mechanism are shown in Figs. 11, 13, and 15. Arrow thicknesses are proportional to the flux of carbon atoms integrated over the flame zone. Next to each reaction path, the reaction partner(s) are written in decreasing order of importance.

For the small fraction of agent which is predicted to react in the flame containing CF_4, the reaction pathways of the CF_3 radical are similar to those in the CHF_3 inhibited flame in most respects. The one exception was that very small amounts of C_2 hydrofluorocarbons were produced, due to most of the agent consumption taking place after the methyl radical had disappeared, giving the reaction

$$CH_3 + CF_3 = CH_2CF_2 + HF, \qquad (R16)$$

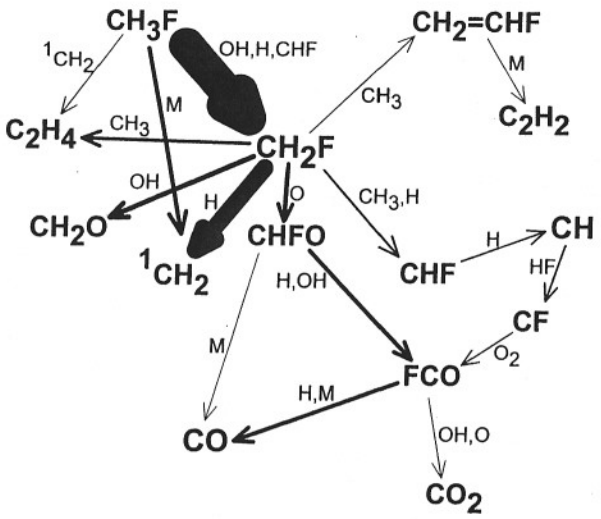

Fig. 10. Reaction pathways of fluorocarbon species in the $CH_4/O_2/CH_3F$ flame according to the base mechanism. Arrow thicknesses are proportional to the carbon atom flux. The most important reaction partner(s) are written next to each arrow in decreasing order of importance.

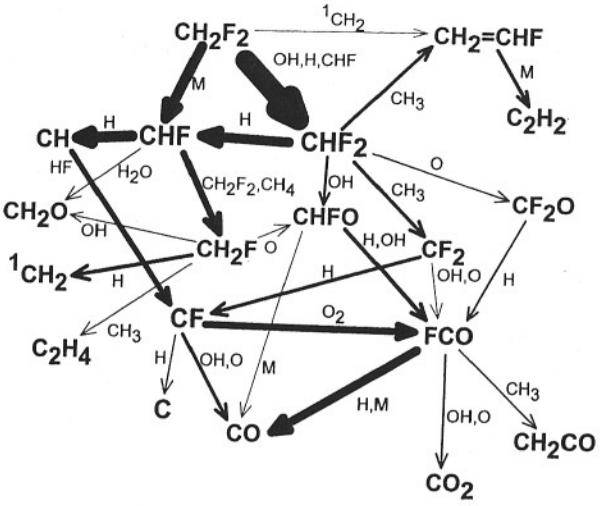

Fig. 12. Reaction pathways of fluorocarbon species in the $CH_4/O_2/CH_2F_2$ flame according to the base mechanism. Arrow thicknesses are proportional to the carbon atom flux.

a very low flux due to the lack of spatial overlap in the profiles of the two reactants.

The modifications made to the mechanism are summarized in Table 4. The revised mechanism gives very good predictions of profiles and relative concentrations for most species. The profiles of CHF appear about 3 mm later than the experiment indicates; however, the experimental difficulties of spectral interference and temperature correction make this disagreement of marginal significance. The calculated CF profiles are about 2 mm too far from the burner. Since the CF spectrum is well characterized and has little interference, this discrepancy is statistically significant. Additional data on the formation and removal kinetics of CF at high temperatures are probably needed to correct this disagreement.

The H atom profiles deviate from the prediction in the postflame zone (>2 cm above the burner). Specifically, the experimental H atom mole fraction begins to decrease while the calculation predicts an increase over the entire compu-

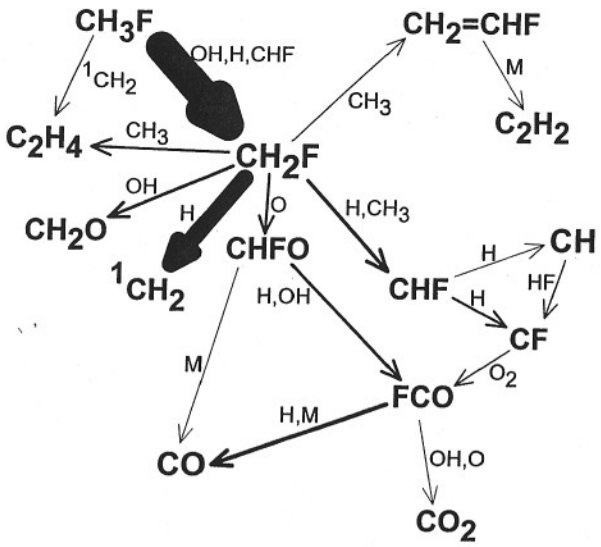

Fig. 11. Reaction pathways of fluorocarbon species in the $CH_4/O_2/CH_3F$ flame according to the revised mechanism. Arrow thicknesses are proportional to the carbon atom flux.

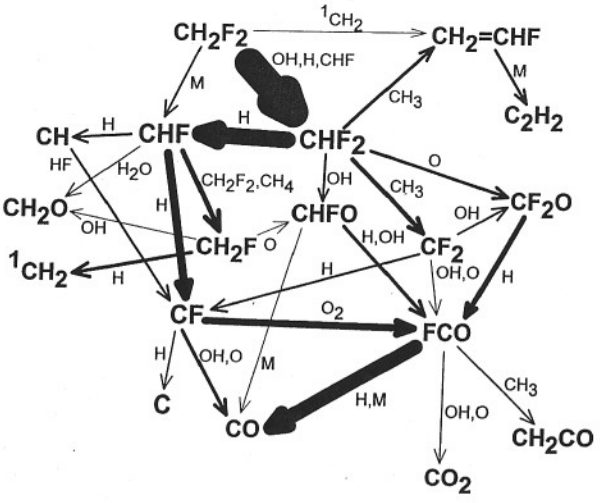

Fig. 13. Reaction pathways of fluorocarbon species in the $CH_4/O_2/CH_2F_2$ flame according to the revised mechanism. Arrow thicknesses are proportional to the carbon atom flux.

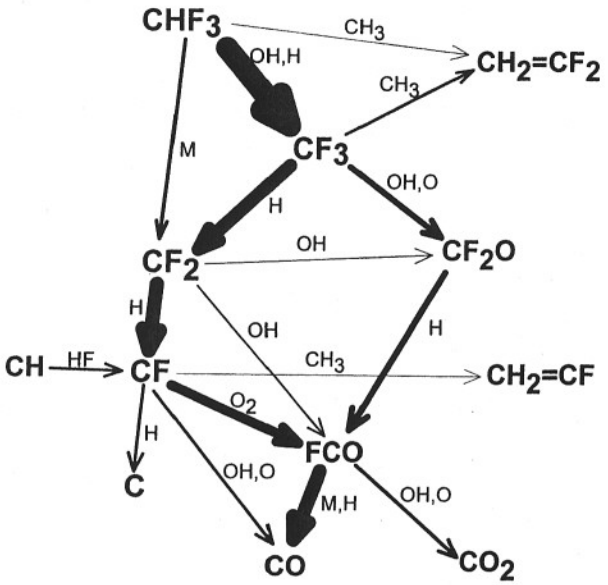

Fig. 14. Reaction pathways of fluorocarbon species in the $CH_4/O_2/CHF_3$ flame according to the base mechanism. Arrow thicknesses are proportional to the carbon atom flux.

tational domain. This behavior is generally seen in this type of burner geometry [33, 54, 55] in all types of flame systems and therefore does not depend on the fluorine chemistry. It may be a consequence of preferential lateral diffusion depleting the H atom mole fraction when the height above the burner becomes comparable to the burner radius. This phenomenon is not likely due to radial spread of the flame with height above the burner, since the mole fraction of OH (which has a much lower diffusivity) is quite accurately predicted by the model up to 5 cm.

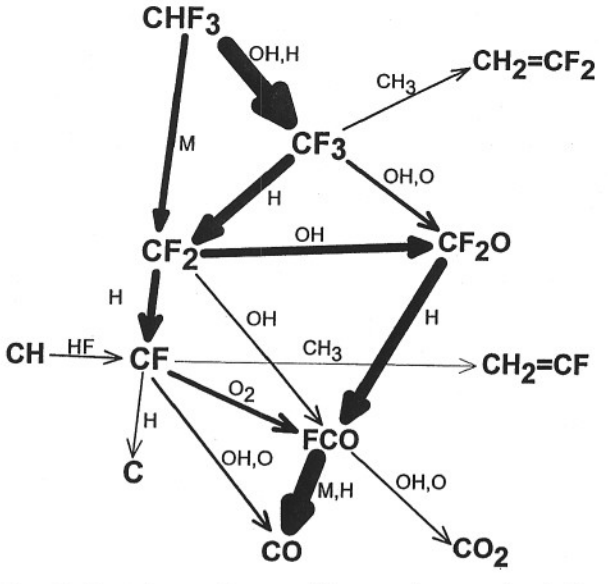

Fig. 15. Reaction pathways of fluorocarbon species in the $CH_4/O_2/CHF_3$ flame according to the revised mechanism. Arrow thicknesses are proportional to the carbon atom flux.

Flame Speed Validation of Revised Mechanism

The HFC mechanism has already been shown to accurately predict the propagation speed of atmospheric pressure methane/air flames containing CH_2F_2 under most conditions [11]. Furthermore, the modifications of Saso et al. produced good agreement with experimental data for methane/air flames containing CHF_3. Since our proposed changes to the kinetics have been dictated by low pressure experiments, it is necessary to make sure that these changes maintain agreement with the atmospheric pressure flame speed data. Several of the reactions we have adjusted were identified in the study of Linteris and Truett as having significant sensitivities for flame speeds.

We performed calculations to compute burning velocities of freely propagating atmospheric pressure flames containing di- or tri-fluoromethane for eight representative conditions for which experimental data are available. The reactant mixtures were composed of methane, air, and inhibitor with ratios of methane/oxygen of 0.45, 0.5, and 0.55, corresponding to equivalence ratios of 0.9, 1.0, and 1.1 for the uninhibited flames. The mixtures contained the agents CH_2F_2 or CHF_3 at up to 7% mole fraction.

The flame speed calculations were performed on a domain extending 25 cm from the flame on the cold boundary and 60 cm on the hot boundary. The calculations used multicomponent viscosities, thermal diffusivities for H and H_2, and windward differencing on the convective term. The initial temperature of the fresh gases was set to 298.2K. Meshes were refined until tolerances of 0.1 and 0.2, respectively, for GRAD and CURV, were satisfied, or until a maximum of 150 grid points was reached. The final meshes contained approximately 120 grid points for the uninhibited methane/air flames and >140 grid points for the inhibited flames.

Results of the atmospheric pressure flame speed calculations are summarized in Table 5. In Figs. 16 and 17, the calculated flame speeds for $CH_4/O_2/CHF_3$ and $CH_4/O_2/CH_2F_2$ mixtures,

TABLE 4

Adjustments to Base Fluorine Mechanism*

Reaction		Arrhenius Parameters $k = AT^b \exp(-E_a/RT)$ A (cm, mol, s)	b	E_a (cal/mol)	Remarks
MD1.	CH_3F (+M) = $^1CH_2$ + HF (+M)				
	High-pressure limit:	1.00E+14	0.0	85,000.	[44]
	Low-pressure limit:	1.50E+16	0.0	67,499.	[44]
	Third body efficiencies: H_2:2.0 H_2O:9.0 CH_4:2.0 CO:1.5 CO_2:2.0 C_2H_6:3.0 CH_3F:6.0 CH_2F_2:6.0 CHF_3:6.0 HF:2.0				
MD4.	CHF + HF + M = CH_2F_2 + M	3.04E+26	−3.26	4060.	
	Third body efficiencies: H_2:2.0 H_2O:9.0 CH_4:2.0 CO:1.5 CO_2:2.0 C_2H_6:3.0 CH_3F:6.0 CH_2F_2:6.0 CHF_3:6.0 HF:2.0				
MD7.	CHF_3 + M = CF_2 + HF + M	3.41E+30	−4.00	69,050.	
	Third body efficiencies: H_2:2.0 H_2O:9.0 CH_4:2.0 CO:1.5 CO_2:2.0 C_2H_6:3.0 CH_3F:6.0 CH_2F_2:6.0 CHF_3:6.0 HF:2.0				
MD8.	CF_4 + M = CF_3 + F + M	9.00E+34	−4.64	122,400	[56]
	Third body efficiencies: H_2:2.0 H_2O:9.0 CH_4:2.0 CO:1.5 CO_2:2.0 C_2H_6:3.0 CH_3F:6.0 CH_2F_2:6.0 CHF_3:6.0 CF_4:6.0				
MD9.	CH_2F + H = $^1CH_2$ + HF	1.10E+14	0.0	0	
MD10.	CH_2F + H = CHF + H_2	5.00E+13	0.0	0	
MA3.	CHF_3 + H = CF_3 + H_2	3.76E+13	0.0	13,100	[12]
NN8.	CHF_2 + OH = CHFO + HF	1.00E+13	0.0	0	
NN21.	CF_2 + O = FCO + F	1.20E+13	0.0	0	
NN23.	CF_2 + OH = CF:O + HF	1.00E+13	0.0	0	
NN25.	CF_2 + OH = CF_2O + H	4.00E+13	0.0	0	
NN30.	CHF + H = CH + HF	6.50E+13	0.0	0	
NN30a.	CHF + H = CF + H_2	2.30E+14	0.0	0	Added channel
NN31.	CF_2 + H = CF + HF	2.35E+13	0.0	0	
NN40.	CF + O = CO + F	8.00E+13	0.0	1410	
NN41.	CF + OH = CO + HF	8.00E+13	0.0	1410.	
NN43.	CH + HF = CF + H_2	2.00E+13	0.0	0	
NN44.	CF + H = C + HF	8.00E+13	0.0	0	
NN51.	CF_2 + M = CF + F + M	6.00E+26	−2.85	106,000	[57]
	Third body efficiencies: H_2O:6.0 CH_4:2.0 CO:1.5 CO_2:2.0 C_2H_6:3.0 CH_3F:6.0 CH_2F_2:6.0 CHF_3:6.0 CF_4:6.0 HF:2.0				
PP27.	CO + F + M = FCO + M	3.09E+19	−1.40	−487	[12]
	Third body efficiencies: H_2:2.0 H_2O:18.0 CH_4:2.0 CO:1.5 CO_2:2.0 C_2H_6:3.0				
PP29.	FCO + H = CO + HF	2.50E+13	0.0	0	[12]
ED45.	CH_3 + CH_2F = C_2H_4 + HF	1.85E+19	−1.86	1870.	
ED47.	CH_3 + CHF_2 = CH_2CHF + HF	1.30E+15	−0.586	634.	
EC3.	CHF_2 + CH_2F = CH_2F_2 + CHF	1.00E+13	0.0	4400.	
EC5.	CH_3 + CHF_2 = CH_4 + CF_2	2.50E+13	0.0	800.	
JD1.	CH_2CHF (+M) = C_2H_2 + HF (+M)				
	High-pressure limit:	1.00E+14	0.0	70,800.	
	Low-pressure limit:	4.20E+15	1.0	70,800.	
	Third body efficiencies: H_2:2.0 H_2O:6.0 CH_4:2.0 CO:1.5 CO_2:2.0 C_2H_6:3.0 CH_3F:6.0 CH_2F_2:6.0 CHF_3:6.0 HF:2.0				
JD2.	CH_2CF_2 (+M) = C_2HF + HF (+M)				
	High-pressure limit:	2.50E+14	0.0	86,000.	
	Low-pressure limit:	9.00E+15	1.0	86,000.	
	Third body efficiencies: H_2:2.0 H_2O:6.0 CH_4:2.0 CO:1.5 CO_2:2.0 C_2H_6:3.0 CH_3F:6.0 CH_2F_2:6.0 CHF_3:6.0 HF:2.0				

TABLE 4

Continued

Reaction		Arrhenius Parameters $k = AT^b \exp(-E_a/RT)$ A (cm, mol, s)	b	E_a (cal/mol)	Remarks
JD3.	CHFCHF[Z] (+M) = C_2HF + HF (+M)				
	High-pressure limit:	2.50E+14	0.0	78,000.	
	Low-pressure limit:	9.00E+15	1.0	78,000.	
	Third body efficiencies: H_2:2.0 H_2O:6.0 CH_4:2.0 CO:1.5 CO_2:2.0 C_2H_6:3.0 CH_3F:6.0 CH_2F_2:6.0 CHF_3:6.0 HF:2.0				
JD4.	CHF = CF_2 (+M) = C_2F_2 + HF (+M)				
	High-pressure limit:	2.50E14	0.0	100,000.	
	Low-pressure limit:	9.00E15	1.0	100,000.	
	Third body efficiencies: H_2:2.0 H_2O:6.0 CH_4:2.0 CO:1.5 CO_2:2.0 C_2H_6:3.0 CH_3F:6.0 CH_2F_2:6.0 CHF_3:6.0 HF:2.0				

* Reaction numbers refer to [8].

respectively, are plotted normalized by the uninhibited flame speed at the same CH_4/O_2 ratio. The experimental data of Linteris and Truett [11] and of Saso et al. [12] are plotted for comparison. The agreement of the calculations with the experimental data is very good for CHF_3. The agreement is less good for the flames containing CH_2F_2 under some conditions. At 6% CH_2F_2 with a methane/oxygen ratio of 0.50, and 5% CH_2F_2 with a methane/oxygen ratio of 0.55, flame speeds were underpredicted by about 25%. In contrast, the calculated speeds of flames with $CH_4/O_2 = 0.50$ with 5% CH_2F_2, and $CH_4/O_2 = 0.45$ with 5% CH_2F_2, were in good agreement with the measurements of Linteris and Truett.

The two conditions for which the mechanism gave poor predictions of the flame speed were both substantially fuel rich, having equivalence ratios of approximately 1.3 (taking into account the effect of the agent on the flame stoichiometry). By contrast, the CHF_3 inhibited flames for which burning velocity data is available all have equivalence ratios less than 1.2. The source of the difficulty in predicting the difluoromethane

TABLE 5

Test Cases for Flame Speed Calculations Using Revised Mechanism ([8] modified according to Tables 3 and 4)

Agent	CH_4/O_2 ratio	Agent mole fraction	Equivalence ratio	Flame speed (cm/s)
None	0.45	—	0.90	35.25
None	0.50	—	1.00	39.37
None	0.55	—	1.10	40.11
CHF_3	0.45	4.04%	1.01	21.57
CHF_3	0.50	5.00%	1.11	19.20
CHF_3	0.50	7.11%	1.15	13.85
CHF_3	0.55	5.19%	1.20	16.27
CH_2F_2	0.45	5.05%	1.16	22.37
CH_2F_2	0.50	5.00%	1.24	18.13
CH_2F_2	0.50	6.00%	1.29	12.88
CH_2F_2	0.55	5.00%	1.33	11.86

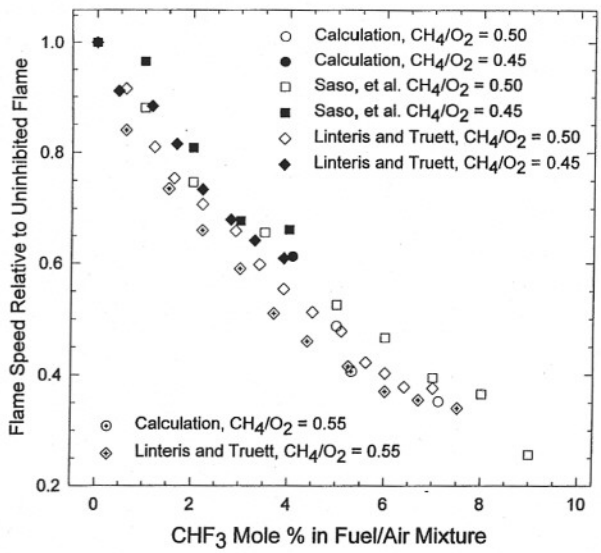

Fig. 16. Comparison of experimental flame speed measurements [11, 12] for CH_4/air/CHF_3 flames with calculations using the revised mechanism.

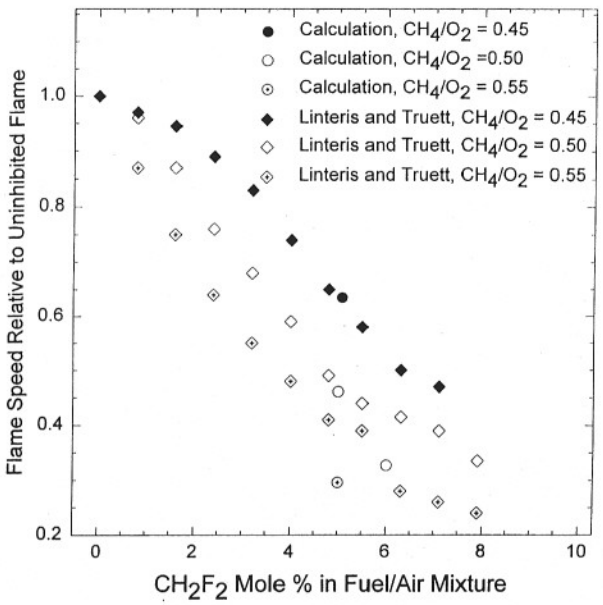

Fig. 17. Comparison of experimental flame speed measurements [11] for CH_4/air/CH_2F_2 flames with calculations using the revised mechanism.

flame speeds must involve fluorine chemistry, since both the study of Linteris and Truett and the validation tests of the GRI mechanism found good agreement with experimentally measured flame speeds for methane/air (uninhibited) flames at these equivalence ratios.

Our modifications did not substantially alter the mechanism's performance for the CH_2F_2 flames from that reported by Linteris and Truett, who also observed substantial underpredictions of flame speeds for rich conditions. Sensitivity analysis of the flame speed for the flame with the methane/oxygen ratio of 0.55 and 5% CH_2F_2 found that the fluorinated reactions having the highest sensitivity coefficients for the flame speed were the agent thermal decomposition and reactions with H and OH, the same as for leaner stoichiometries. Reactions involving fluoromethyl + (fluoro)methyl including recombination and hydrogen disproportionation had sensitivities about an order of magnitude lower (absolute values of 0.005 compared to 0.05 for the difluoromethane removal reactions; the $H + O_2 = OH + O$ reaction has a sensitivity of 0.5, the highest value in the inhibited as well as the uninhibited flames). For a reaction having a sensitivity coefficient of X for the flame speed, a 1% increase in the reaction's kinetic rate will cause an X% change in the flame speed, a positive sensitivity coefficient corresponding to an increased flame speed. The recombination of two (fluoro)methyl radicals to form an ethylene with HF elimination had a positive sensitivity coefficient, while hydrogen disproportionation to form a (fluoro)methane and a (fluoro)carbene had a negative sensitivity coefficient. Alterations to the kinetics of the C_2 reactions are probably needed to correctly predict flame speeds under rich conditions, but such changes cannot be validated without additional data. Species profiles for rich stoichiometries (ideally comprising some C_2 species as well as those monitored here) are needed to ascertain which aspects of the kinetics need attention.

Conclusions

We have obtained profiles for a number of intermediate species in methane/oxygen flames containing C_1 hydrofluorocarbons and propose chemically plausible adjustments to selected reactions in the HFC mechanism. This revised mechanism provides good agreement with both our low-pressure profile data and, except for rich stoichiometries, atmospheric pressure flame speeds. In making changes to the kinetic mechanism, it must be emphasized that because of the large number of kinetic parameters, which could conceivably be modified and the rather limited range of data, there is not a unique set of adjustments that will adequately reproduce the experimental results. Having information on oxygen containing fluorine species and on C_2 species would be very useful in diagnosing further uncertainties in the mechanism, which include the relative reactivities of the fluorinated radicals with O, H, and OH, and the rather poor prediction of flame speeds under rich stoichiometries. Flame speed data on methane/air/CH_3F mixtures, while not of practical importance for fire suppression, would add to the data needed to interrogate hydrofluorocarbon kinetics. The profiles obtainable for the CHF radical could benefit from investigation of alternative wavelengths for a fluorescence diagnostic and especially from an improved temperature correction. Individual reactions in the HFC mechanism, which, based on our study, appear to require attention include the product

channels of atomic hydrogen reactions with fluorinated radicals (H_2 vs HF product), and the falloff behavior and particularly the third body efficiencies of flame species for thermal decomposition reactions.

We thank Phillip Westmoreland and Don Burgess for helpful discussions. This work was funded by the U.S. Naval Sea Systems Command.

REFERENCES

1. *Scientific Assessment of Ozone Depletion: 1994*, WMO Global Ozone Research and Monitoring Project-Report No. 37, World Meteorological Organization, Geneva, 1995.
2. Miziolek, A. W., and Tsang, W., eds., *Halon Replacements: Technology and Science*, ACS Symposium Series 611, American Chemical Society, Washington, 1994.
3. Westbrook, C. K., *Combust. Sci. Technol.* 34:201–225 (1983).
4. Sheinson, R. S., Penner-Hahn, J. E., and Indritz, D., *Fire Safety J.* 15:437–450 (1989).
5. Nyden, M. R., Linteris, G. T., Burgess, Jr., D. R. F., Westmoreland, P. R., Tsang, W., and Zachariah, M. R., in *Evaluation of Alternative In-Flight Fire Suppressants for Full-Scale Testing in Simulated Aircraft Engine Nacelles and Dry Bays*, Grosshandler, W. L., Gann, R. G., and Pitts, W. M., eds. NIST SP 861 (1994), pp. 467–642.
6. Burgess, Jr., D. R. F., Zachariah, M. R., Tsang, W., and Westmoreland, P. R., *Thermochemical and Chemical Kinetic Data for Fluorinated Hydrocarbons*, NIST Technical Note 1412, NIST, Gaithersburg, MD., 1995.
7. Westmoreland, P. R., Burgess, Jr., D. R. F., Zachariah, M. R., and Tsang, W., *Twenty-Fifth Symposium (International) on Combustion*, The Combustion Institute, Pittsburgh, 1994, pp. 1505–1511.
8. Burgess, Jr., D. R. F., Zachariah, M. R., Tsang, W., and Westmoreland, P. R., *Prog. Energy Combust. Sci.* 21:453 (1996).
9. The current NIST HFC mechanism may be downloaded from http://fluid.nist.gov/ckmech.html.
10. Noto, T., Babushok, V., Burgess, Jr., D. R. F., Hamins, A., Tsang, W., and Miziolek, A., *Twenty-Sixth Symposium (International) on Combustion*, The Combustion Institute, Pittsburgh, 1996, pp. 1377–1383.
11. Linteris, G. T., and Truett, L., *Combust. Flame* 105: 15–27 (1996).
12. Saso, Y., Zhu, D. L., Wang, H., Law, C. K., and Saito, N., *Combust. Flame* 114:457–468 (1998).
13. Linteris, G. T., Burgess, Jr., D. R., Babushok, V., Zachariah, M., Tsang, W., and Westmoreland, P., *Combust. Flame* 113:164–180 (1998).
14. Papas, P., Fleming, J. W., Sheinson, R. S., *Twenty-Sixth Symposium (International) on Combustion*, The Combustion Institute, Pittsburgh, 1996, pp. 1405–1411.
15. Fallon, G. S., Chelliah, H. K., and Linteris, G. T., *Twenty-Sixth Symposium (International) on Combustion*, The Combustion Institute, Pittsburgh, 1996, pp. 1395–1403.
16. McNesby, K. L., Daniel, R. G., Modiano, S. H., and Miziolek, A. W., *Proceedings of the Halon Options Technical Working Conference*, Albuquerque, NM, May 7–9, 1996, pp. 295–305.
17. Babushok, V., Burgess, Jr., D. F. R., Linteris, G. T., Tsang, W., and Miziolek, A. W., *Proceedings of the Halon Options Technical Working Conference*, Albuquerque, NM, May 9–11, 1995, pp. 239–250.
18. Brabson, G. D., Walters, E. A., Schiro, J., Spencer, C., Tapscott, R. E., and Patterson, R. A., *Proceedings of the Halon Options Technical Working Conference*, Albuquerque, NM, May 7–9, 1996, pp. 213–222.
19. Vandooren, J., Nelson da Cruz, F., and Van Tiggelen, P. J., *Twenty-Second Symposium (International) on Combustion*, The Combustion Institute, Pittsburgh, 1988, pp. 1587–1595.
20. Sanogo, O., Delfau, J.-L., Akrich, R., and Vovelle, C., *Twenty-Fifth Symposium (International) on Combustion*, The Combustion Institute, Pittsburgh, 1994, pp. 1489–1496.
21. Womeldorf, C., Grosshandler, W., and King, M., *Proceedings of the 1996 Fall Technical Meeting of the Eastern States Section of the Combustion Institute*, Hilton Head, SC, Dec. 9–11, 1996, pp. 257–260.
22. Berry, R. J., Ehlers, C. J., Burgess, D. R., Zachariah, M. R., and Marshall, P., *Chem. Phys. Lett.* 269:107–116 (1997).
23. Fleming, J. W., Burton, K. A., and Ladouceur, H. D., *Chem. Phys. Lett.* 175:395–400 (1990).
24. Williams, B. A., and Fleming, J. W., *Combust. Flame* 98:93–106 (1994).
25. L'Espérance, D., Williams, B. A., and Fleming, J. W., *Chem. Phys. Lett.* 280:113–118 (1997).
26. Kee, R. J., Grcar, J. F., Smooke, M. D., and Miller, J. A., *Sandia Report SAND85-8240*, 1985.
27. Kee, R. J., Rupley, F. M., and Miller, J. A., *Sandia Report SAND89-8009*, 1989.
28. Kee, R. J., Warnatz, J., and Miller, J. A., *Sandia Report SAND83-8209*, 1983.
29. Bowman, C. T., Hanson, R. K., Gardiner, W. C., Lissianski, V., Frenklach, M., Goldenberg, M., and Smith, G. P., *GRI-Mech 2.11—An Optimized Detailed Chemical Reaction Mechanism for Methane Combustion and NO Formation and Reburning*, GRI Report GRI-97/0020, 1997, Gas Research Institute, Chicago. http://www.ME.Berkeley.edu/gri_mech/
30. Williams, B. A., and Fleming, J. W., *Combust. Flame* 110:1–13 (1997).
31. Gaydon, A. G., *The Spectroscopy of Flames*, Chapman & Hall, London, 1957.
32. Devriendt, K., Van Look, H., Ceursters, B., Peeters, J., *Chem. Phys. Lett.* 261:450–456 (1996).
33. Williams, B. A., and Fleming, J. W., *Combust. Flame* 100:571–590 (1995).
34. Goldsmith, J. E. M., and Laurendeau, N. M., *Opt. Lett.* 15:576–578 (1990).
35. Dieke, G. H., and Crosswhite, H. M., *J. Quant. Spectry. Radiative Transfer* 2:97 (1962).
36. Griffiths, J. F., and Barnard, J. A., *Flame and Com-*
37.
38.
39.
40.
41.
42.
43.
44.
45.
46.
47.

bustion, Blackie Academic and Professional, Glasgow, UK, 1995, pp. 102–109.
37. Rensberger, K. J., Jeffries, J. B., Copeland, R. A., Kohse-Höinghaus, K., Wise, M. L., and Crosley, D. R., *Applied Optics* 28:3556–3566 (1989).
38. Ashfold, M. N. R., Castano, F., Hancock, G., and Ketley, G. W., *Chem. Phys. Lett*. 73:421–424 (1980).
39. Sappey, A. D., Crosley, D. R., and Copeland, R. A., *Appl. Phys. B*. 50:463 (1990).
40. Porter, T. L., Mann, D. E., and Acquista, N., *J. Mol. Spectr*. 16:228–263 (1965).
41. Booth, J.-P., Hancock, G., Toogood, M. J., and McKendrick, K. G., *J. Phys. Chem*. 100:47–53 (1996).
42. Douglass, C. H., Williams, B. A., and McDonald, J. R., *Combust. Flame* 107:475–478 (1996).
43. Hidaka, Y., Nakamura, T., and Kawano, H., *Chem. Phys. Letters* 187:40–44 (1991).
44. Schug, K. P., Wagner, H. Gg., *Z. Chem. Phys*. 86:59–66 (1973).
45. Simmie, J. M., Quiring, W. J., and Tschuikow-Roux, E., *J. Phys. Chem*. 74:992–994 (1970).
46. Simmie, J. M., and Tschuikow-Roux, E., *J. Phys. Chem*. 74:4075–4079 (1970).
47. Tsai, C.-P., and McFadden, D. L., *J. Phys. Chem*. 94:3298 (1990).
48. Clark, D. T., and Tedder, J. M., *Trans. Faraday Soc*. 62:399 (1966).
49. Tsai, C.-P., and McFadden, D. L., *J. Phys. Chem*. 93:2471 (1989).
50. Tsai, C.-P., and McFadden, D. L., *Chem. Phys. Lett*. 173:241–244 (1990).
51. Biordi, J. C., Lazzara, C. P., and Papp, J. F., *J. Phys. Chem*. 80:1042–1048 (1976).
52. Biordi, J. C., Lazzara, C. P., and Papp, J. F., *J. Phys. Chem*. 82:125 (1978).
53. Van Hoeymissen, J., De Boelpaep, I., Uten, W., and Peeters, J., *J. Phys. Chem*. 98:3725–3731 (1994).
54. Bernstein, J. S., Fein, A., Choi, J. B., Cool, T. A., Sausa, R. C., Howard, S. L., Locke, R. J., and Miziolek, A. W., *Combust. Flame* 92:85–105 (1993).
55. Heard, D. E., Jeffries, J. B., Smith, G. P., and Crosley, D. R., *Combust. Flame* 88:137–148 (1992).
56. Modica, A. P., and Sillers, S. J., *J. Chem. Phys*. 48:3283–3289 (1968).
57. Modica, A. P., *J. Chem. Phys*. 44:1585–1589 (1966).

Received 2 October 1997; revised 17 August 1998; accepted 27 August 1998